Polar distortion in ultrathin $BaTiO_3$ films studied by *in situ* LEED *I-V*

Junsoo Shin,[1,2] V. B. Nascimento,[1] A. Y. Borisevich,[2] E. W. Plummer,[1,3] S. V. Kalinin,[2,3] and A. P. Baddorf[3,*]
[1]*Department of Physics and Astronomy, The University of Tennessee, Knoxville, Tennessee 37996, USA*
[2]*Materials Sciences and Technology Division, Oak Ridge National Laboratory, Oak Ridge, Tennessee 37831, USA*
[3]*Center for Nanophase Materials Sciences, Oak Ridge National Laboratory, Oak Ridge, Tennessee 37831, USA*
(Received 2 April 2008; published 25 June 2008)

Phase stability in nanoscale ferroelectrics is governed by the interplay of electrostatic depolarization energy, domain formation, adsorption, and surface band bending. Using *in situ* low-energy electron-diffraction intensity versus voltage (LEED *I-V*), we have characterized 4 and 10 ML $BaTiO_3$ films, grown using pulsed laser deposition with fully compressive strain on a $SrRuO_3/SrTiO_3$ substrate. LEED *I-V* reveals a single surface dead layer and a monodomain vertically polarized state below. The single orientation is attributed to the intrinsic imprint asymmetry and the stability of a polarized phase to compensation of depolarizing charges by dipoles induced by surface stress.

DOI: 10.1103/PhysRevB.77.245437 PACS number(s): 68.35.B−, 61.05.jh, 68.55.−a, 77.84.−s

I. INTRODUCTION

In ferroelectric materials, discontinuity of the normal component of polarization results in a polarization charge and in an associated depolarization electric field,[1] destabilizing the ferroelectric phase in ultrathin layers. Minimization of the free energy can proceed by antiparallel domain formation,[2] screening by adsorbates,[3] or intrinsic carriers, as observed by local potential measurements[4] and x-ray diffraction.[5] The depolarization field created by an unscreened dimensionally confined ferroelectric can lead to toroidal polarization states[6] or to surface band bending and formation of depletion and accumulation layers.[7,8] The stability of the ferroelectric state ultimately is determined by the efficiency of screening. Remarkably, the minimum ferroelectric film thickness observed has dropped from ~10s of microns in the 1950s to several unit cells recently, reflecting advances in both theory and materials synthesis and characterization.

The ferroelectric distortion in the lead-based compounds such as $PbTiO_3$ and $PbZrO_3$ is typically larger than in alkaline-earth based perovskites such as $BaTiO_3$ and $SrTiO_3$ as Pb atoms participate much more strongly in the ferroelectric distortion. Consequently, lead-based materials have been reported to be polar, as thin as three unit cells.[9] In $BaTiO_3$, a recent experimental upper bound of ~12 unit cells on the thinnest polarized film was established through direct ferroelectric measurement in a capacitor geometry.[10] First-principles theory has predicted polarization in $BaTiO_3$ films as thin as six unit cells[11] or further reduced to three unit cells by polarization in adjacent electrodes.[12] Fabrication of the films free of pinholes over macroscopic length scales required for capacitor fabrication, as well as fabrication of top electrodes *in situ* (required to avoid chemisorption of water on the surfaces and the associated changes in phase stability), represents a problem several orders of magnitude more difficult than *in situ* growth and characterization only. These technological complications preclude direct measurements in ultrathin films.

An additional level of complexity is introduced by atomistic reconstructions of oxide surfaces, which are not considered in by mean-field theories. For cubic perovskites, reconstruction attributed to surface strain results in an intrinsic dipole moment even when the bulk is unpolarized.[13] Surface strain or stoichiometry deviations can result in a broad range of structural reconstructions including antiferrodistortive phase transitions associated with octahedral tilting.[14,15] Nevertheless, experimental studies of ferroelectric surfaces have been limited by their insulating behavior and by sensitivity to contamination. Multicomponent, nonlayered oxides such as ferroelectrics generally do not allow preparation of clean stoichiometric surfaces by cleaving or sputtering annealing,[15] therefore *in situ* growth and characterization are required. To date, only a few *in situ* studies of ferroelectric materials have been reported; these have involved x-ray techniques[9,16] or low-energy electron-diffraction intensity vs voltage (LEED *I-V*).[15,17]

In this work, the structure of the $BaTiO_3$ (100) surface is determined using *in situ* LEED *I-V* (Ref. 18) of ultrathin films. The penetration depth of the low-energy electrons is limited to the first few atomic layers of the surface, providing information on the top three unit cells. Within the top unit cell, atomic positions are determined to be better than 0.1 Å, however, multiple electron scattering in LEED makes surface structure determination a complex search problem associated with a quantitative theory-experimental comparison.[18] Our work underscores the need for *in situ* characterization of oxide ultrathin films and illustrates how surface structure can influence polarization stability in an ultrathin film.

II. EXPERIMENT DETAILS

Heteroepitaxial $BaTiO_3$ films were grown by pulsed laser deposition and were monitored during deposition with differentially pumped reflective high-energy electron diffraction (RHEED) in a locally designed UHV system combining connected chambers for growth and *in situ* characterization by LEED *I-V*. Fully strained epitaxial $BaTiO_3/SrRuO_3$ bilayers were grown on (001)-oriented TiO_2-terminated[19] $SrTiO_3$ substrates using a KrF excimer laser ($\lambda = 248$ nm) with layer thickness monitored by high-pressure RHEED. A 15-nm-thick SrO-terminated[20,21] $SrRuO_3$ film with an atomically flat

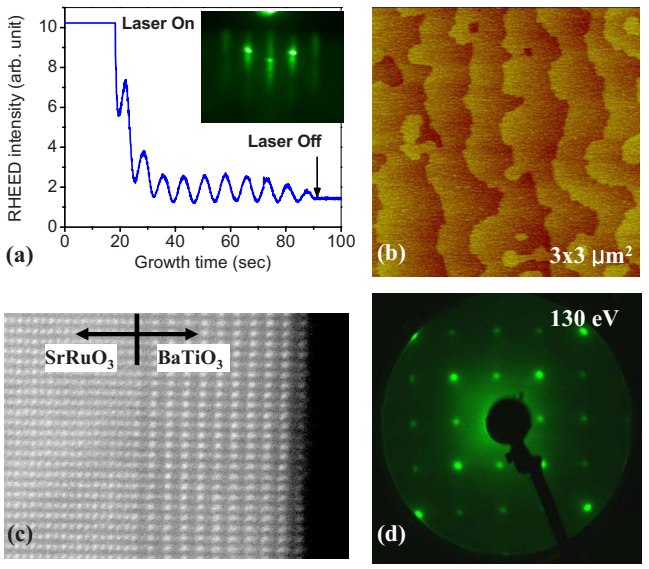

FIG. 1. (Color online) 10 ML thick $BaTiO_3$ films grown on $SrRuO_3/SrTiO_3$: (a) *in situ* RHEED oscillation during deposition and RHEED pattern, (b) *ex situ* AFM topography, (c) cross-sectional *Z* contrast STEM image, and (d) *in situ* (1×1) LEED pattern after deposition.

surface was deposited as a bottom electrode at a substrate temperature of 700 °C in 100 mTorr O_2 with an average deposition flux of 0.05 ML/s,[21,22] followed by growth of ultrathin $BaTiO_3$ films (4 and 10 ML unit cells) at 700 °C in 10 mTorr O_2 and a flux of 0.15 ML/s (Ref. 23). Figure 1(b) shows an *ex situ* atomic force microscopy (AFM) image of the typical film morphology after deposition of $BaTiO_3$ films on $SrRuO_3$ films, which illustrates a stepped topography similar to that of the $SrTiO_3$ substrate. Thicknesses of $BaTiO_3$ films were determined by intensity oscillations [Fig. 1(a)] of a RHEED specular spot during growth, indicating a two-dimensional (2D) layer-by-layer growth mode. Images from cross-sectional *Z* contrast[24] scanning transmission electron microscopy (STEM), such as Fig. 1(c), confirm the thicknesses of $BaTiO_3$ films and demonstrate fully strained films with few dislocations. For electron-diffraction studies, samples were transferred from the growth chamber to the LEED chamber, where ultrahigh-vacuum conditions $(2\times10^{-10}$ Torr) were established, without exposure in air. Typical LEED patterns for 4 and 10 ML thin $BaTiO_3$ films, taken at room temperature, are shown in Fig. 1(d). Sharp (1×1) LEED patterns have been observed in all films at beam energies between 50 and 500 eV, indicating a *P*4*mm* group symmetry of fully strained films.

The LEED *I-V* data for 4 and 10 ML $BaTiO_3$ films were taken at room temperature and were recorded in energy steps of 1 eV with a high-resolution 10-bit digital charge-coupled device (CCD) camera, controlled by the commercial software (V 4.30) from KSA 400. Experimental $I(V)$ curves were extracted from digitized diffraction patterns, smoothed using a five-point least-squares cubic polynomial algorithm and normalized to the electron gun current. Symmetrically equivalent beams, according to the *P*4*mm* symmetry, were then averaged leading to 11 [(1,0), (1,1), (2,0), (2,1), (2,2), (3,0), (3,1), (3,2), (3,3), (4,0), and (5,0)] and 8 [(1,0), (1,1), (2,0), (2,1), (2,2), (3,0), (3,3), and (4,0)] nonequivalent beams and total energy ranges of 2589 and 1719 eV, respectively, for the 4 and 10 ML thin films.

III. LEED *I-V* STRUCTURAL ANALYSIS

Of all surface sensitive structure methods, LEED (Ref. 18) has produced the most well characterized structural models. The penetration depth of low-energy electrons is limited due to their strong interaction with the atoms in the first few atomic layers of the surface (multiple-scattering process), enhancing the surface sensitivity, but complicating a direct inversion of experimental data, instead it requires a quantitative theory-experiment comparison for surface structure determination by LEED. Experimental and theoretical complexity contributes to the existence of only a few works concerning surface crystallography of ferroelectric metal oxides by LEED among the few complete characterizations of any metal oxides. From the experimental point of view, the preparation of a clean, stoichiometric, and geometrically ordered metal oxide surfaces, necessary for the structure determination, is usually a complicated task.[15] Second, LEED makes use of charged particles (electrons) as probes, which constitutes a problem since many interesting oxides are electrical insulators. Theoretical calculations are particularly complicated due to the structural and compositional complexity of most oxides as well as to the effects of charge transfer between the metallic cation and the oxygen anion.[25]

The theory-experiment comparison with LEED *I-V* is made quantitative by the use of a reliability or *R* factor, with the one defined by Pendry (R_P) (Refs. 18 and 26) being the most commonly employed. An R_P equal to zero indicates a perfect correlation between theory and experiment, while a value equal to one indicates that theoretical and experimental $I(V)$ curves are uncorrelated. A final R_P below 0.30 generally indicates that one can be confident in the determined structure, depending on the complexity of the system and the total energy range of the experimental $I(V)$ curves, although published values of R_p have been below 0.1 for simple metal surfaces and above 0.5 for oxide perovskites. The surface structure determination process consists of a search process to locate the global minimum of the *R* factor, which should correspond most closely to the actual structure.

A muffin-tin (MT) potential[27] is employed in the multiple-scattering calculations to describe the individual atoms. In this approach, the potential inside a radial distance from the nucleus (MT radii) is spherically symmetrized and assumes a constant value outside the MT. Due to the spherical symmetry, the scattering from individual atoms can be fully described by phase shifts (the partial-wave method).[27] Phase-shift calculation for metallic systems consists of a straightforward approach, with the MT radii being defined as half the shortest distance between nearest neighbors. However, phase-shift calculation for metal oxides is not an easy task due to the charge transfer that takes place between the metallic cation and the oxygen anion: (1) MT radii definition—the metallic cation will have a smaller radii than the neutral metal specie and O^{-2} will have a larger radii than neutral oxygen. (2) Ionic charge densities—effective ionic

charge densities for both cation and anion must be employed in the potential calculation. A direct consequence of these simplifications is reflected by the large values commonly reported in the literature of the Pendry *R* factor (R_P) for metal oxides, which indicates less agreement between experimental data and calculated diffraction.

Phase-shift calculations for the (001) surface of $BaTiO_3$ were obtained by following a new approach, using the optimized MT potential method.[28] In a recent work this approach has been successfully applied to the structural determination of the (001) surface of the $Ca_{1.5}Sr_{0.5}RuO_4$ layered perovskite.[25] Within the optimized muffin-tin potential approach, the spherical MT wells obtained by the Mattheiss prescription[27] include preassigned surface core-level shifts and are continuously connected with a flat interstitial potential. It is fundamental for the MT optimization that the local electron distribution of MT wells and interstices equilibrate the positive nuclear background charge. To assure equilibrium, the MT radii are optimized at each energy to generate a continuous potential at the MT radii and to avoid undesired scattering resonance features in the phase shifts. The interstitial potential, related to the real part of inner potential V_{0R}, is energy dependent due to the exchange-correlation approach adopted. This optimized MT approach is able to solve two serious problems related to phase-shift generation for metal oxides. The first is avoiding a MT radii definition for the different atomic species, since these parameters are optimized at every energy to assure continuity of the potential. The second is preventing resonance effects due to discontinuities in the potential problem by producing smooth phase shifts for the elements. An important point is that the optimized MT approach also allows the inclusion of an energy dependent real part of the inner potential $[V_{0R}(E)]$. The energy dependent real part of the inner potential plays a key role in the final theory-experiment agreement, particularly in the case of perovskites such as $BaTiO_3$ and $Ca_{1.5}Sr_{0.5}RuO_4$ (Ref. 25). Due to the complex structure of these oxides, the $I(V)$ curves present a high number of peaks (compared to the ones for simple metals), and neglecting the $V_{0R}(E)$ correction in the theoretical calculations induces a systematic error in the diffracted peaks positions. This systematic error not only leads to a high value for the R_P (consequently affecting accuracy) but can even induce errors in the final structure determined.[29,30] By adopting the optimized MT approach, acceptable final R_p values of 0.30 and 0.32 have been obtained for the 4 and 10 ML $BaTiO_3$ thin films, respectively in this work.

Debye temperatures were obtained from x-ray and neutron-diffraction results for tetragonal bulk $BaTiO_3$ (Ref. 31), yielding values of 254, 760, and 490 K for the Ba, O, and Ti, respectively. A total of ten phase shifts were employed in the calculations, as well as a constant imaginary inner potential (V_{0I}) equal to −6.0 eV. The full dynamic LEED calculations were performed using the symmetrized automated tensor LEED code (SATLEED) (Ref. 32), modified to include the energy dependence of the real part of the inner potential $[V_{0R}(E)]$ (Ref. 25).

The first step in surface structure optimization was to determine the tetragonal lattice parameters $\boldsymbol{a}$ (in plane) and $\boldsymbol{c}$ (out of plane) for the 4 and 10 ML thin films as modified from the bulk by substrate and film thickness.[33] Next, six different structural models have been explored for Ba-O terminations: (a) no ferroelectric polarization, with a bulk terminated surface, (b) no ferroelectric polarization, with surface structure optimization, (c) upward (out of surface) ferroelectric polarization, with a bulk terminated surface, (d) upward ferroelectric polarization, with an optimized surface structure, (e) downward (into surface) ferroelectric polarization, with a bulk terminated surface, and (f) downward ferroelectric polarization, with an optimized surface structure. The ferroelectric displacements of the atoms inside the unit cell, adopted in cases (c), (d), (e), and (f), were defined to be proportional to the $\boldsymbol{c}$ lattice parameter, keeping the same ratio observed in bulk tetragonal $BaTiO_3$ (Ref. 31). The results for the 10 ML system are shown in Fig. 2. Note that only the upward polarization cases [(c) and (d)] lead to an acceptable solution, with the R_P global minima found in the same region of the parameters space. A small difference is observed in the optimal values for the $\boldsymbol{a}$ lattice parameter, but the LEED technique has a low sensitivity to in-plane structural parameters.[18] The global minimum for case (d) is relatively deep with a moderate R_P value (0.34), indicative of the veracity of this model. The R_P minimum observed in case (b) [no polarization, with optimized surface structure] corresponds to the first Ti atom above the O plane, i.e., with surface ferroelectric polarization and in agreement with (c) and (d) cases. The $R_P(\boldsymbol{a},\boldsymbol{c})$ contour plot for case (a) [no polarization, bulk terminated surface] presents two shallow minima (R_P=0.64), with the higher value corresponding to an unrealistic value for the real part of the inner potential. In the cases in which a downward polarization was explored [(e) and (f)], no minimum is observed on the $R_P(\boldsymbol{a},\boldsymbol{c})$ surface. The grid search results indicate an upward polarization of the 10 ML $BaTiO_3$ film. Similar results were obtained for the 4 ML system.

IV. FILM STRUCTURE: RESULTS AND DISCUSSION

A summary of the results obtained for the 10 ML film are presented in Fig. 3. The quality of fit, R_P, is shown as a function of the number of top $BaTiO_3$ unit cells assumed with upward and downward polarization. In every case, optimal values for *a* and *c* have been employed and the vertical displacements of the atoms within the top unit cells (assumed with polarization) have been optimized. As it can be seen, the best theory-experiment agreement is achieved for the case of upward polarization and poor agreement for downward polarization. It can also be seen that R_p is minimized with at least $2\sim3$ upward polarized unit cells in the surface of the thin films. Similar results were found for the 4 ML system.

The optimized in-plane *a* lattice parameter ($\sim$0.391 nm) reveals that the films are compressively fully strained, i.e., they have adopted the substrate lattice constant, which is consistent with TEM and RHEED observations. Structural models adopting a surface terminated with a Ti-O_2 layer have also been investigated and excluded by inadequate LEED *I-V* theory-experiment agreement as well as by RHEED and cross-section TEM results. Even though the

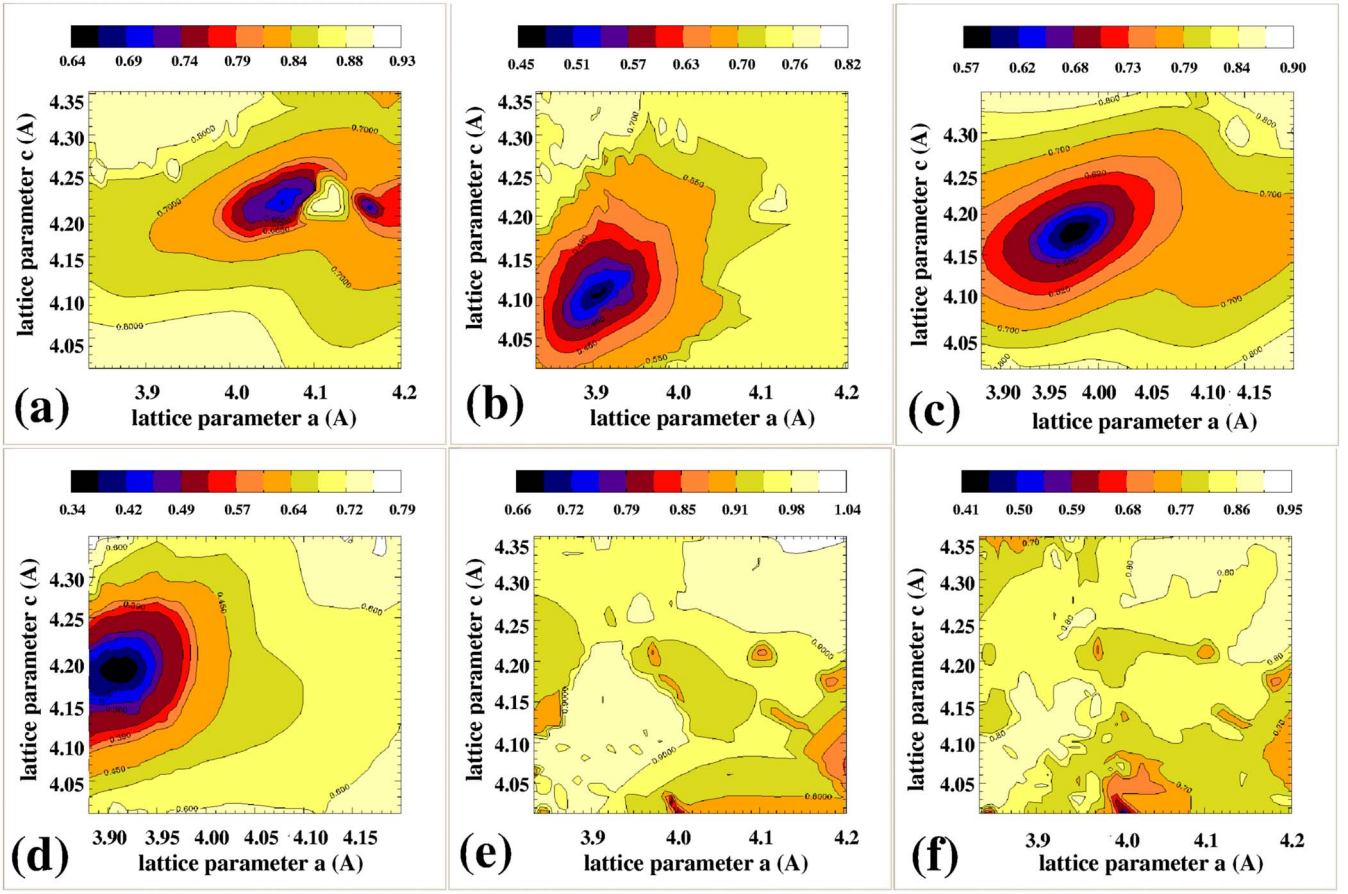

FIG. 2. (Color online) Pendry *R* factor as a function of ***a*** and ***c*** lattice parameters for the 10 ML system. Six different situations have been explored: (a) no polarization and no surface structure optimization, (b) no polarization with surface structure optimization, (c) upward polarization without surface structure optimization, (d) upward polarization with surface structure optimization, (e) downward polarization without surface structure optimization, and (f) downward polarization with surface structure optimization.

films are fully strained, oxygen vacancies could be a predominant source of point defects in these films, which would reduce ferroelectricity. Generally, diffraction methods such as LEED *I-V* are insensitive to vacancies below a few atomic percent, while above ~1% vacancies will destabilize the perovskite structure due to the formation of crystallographic shear planes. However, as a check of the structural refinement results, we have performed LEED *I-V* refinement vary-

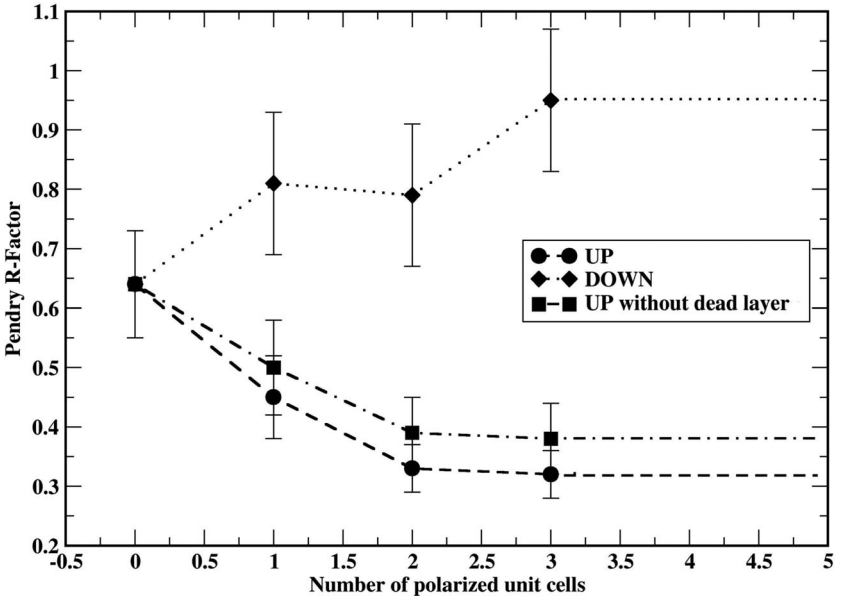

FIG. 3. Pendry *R* factor as a function of the number of $BaTiO_3$ unit cells assumed with upward and downward polarization. The Pendry *R* factor as a function of the number of upward polarized unit cells is also presented without the presence of the top Ba-O dead layer, for comparison.

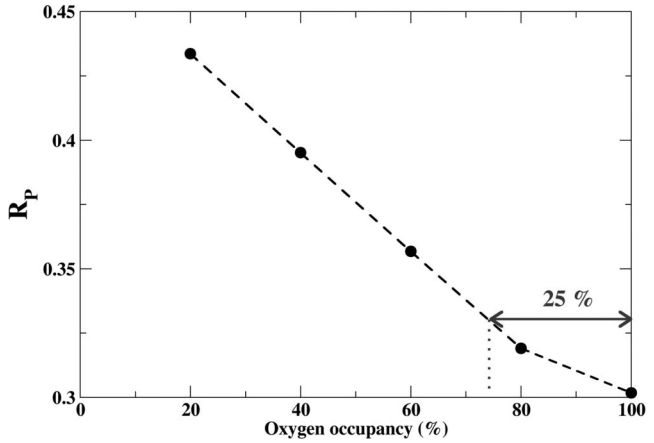

FIG. 4. Pendry *R* factor as a function of the top oxygen layer occupancy, as obtained for the 4 ML LEED data set.

ing the occupancy of the oxygen sites. The results obtained by the LEED, within our accuracy (±25%), do not indicate the presence of oxygen deficiencies, as shown in Fig. 4.

To illustrate the sensitivity of LEED *I-V* to the ferroelectric distortions in these films, Fig. 5 presents a comparison between theoretical $I(V)$ curves generated for cubic $BaTiO_3(001)$ in five distinct configurations: Ti centered (no displacement), Ti up (0.06 Å), Ti down (0.06 Å), uncorrelated Ti up and down domains (0.06 Å, 50%, and 50%), and a (2×2) structure with up and down Ti displacements (0.06 Å). As can be seen, the theoretical $I(V)$ curves are very sensitive to the Ti displacements in different configurations.

Once the basic structural model was established, in this case an upward displacement of Ti in a fully strained film, the (001) surface structural parameters of both 4 and 10 ML systems were optimized. In the structural search, the atoms of the two topmost perovskite layers were displaced only vertically (for a total of ten structural parameters), to maintain the observed *P4mm* symmetry. Considering the complexity of the $BaTiO_3$ structure, acceptable final theory-experiment agreement has been obtained for both 4 and 10 ML systems, as characterized by the final R_P values of 0.30 and 0.32, respectively. The comparisons between theoretical and experimental $I(V)$ curves are shown in Fig. 6. A schematic presentation of the final structures obtained for both 4 and 10 ML systems can be seen in Fig. 7. Optimal structural parameters values for both systems are presented in Table I, according to the scheme defined in Fig. 7. Table II presents the values for the ferroelectric distortions[13,34] for each layer involved in the surface structure optimization. The ferroelectric distortion (δ_{FE}) is defined as the internal rumple in the Ba-O and Ti-O_2 layers, in units of the lattice constant *c*, and it can be used to qualitatively evaluate the polarization. The ferroelectric distortion (δ_{FE}) is positive if the metallic cations are above the oxygen anions.

The structural results presented in Table II, within uncertainties, indicate a lack of polarization in the top Ba-O layer, which has little internal rumple. A plot of R_p versus the number of upward polarized unit cells without the existence of the dead layer is presented in Fig. 3. Although considerable uncertainties are associated with the existence of this dead layer (see Fig. 3), the structural results obtained for both 4 and 10 ML systematically point to its existence. Below this top dead layer, from the first Ti-O_2 layer on, the atomic displacements associated with upward polarization are present both in Ba-O and Ti-O_2 layers (Fig. 3). These results indicate the presence of upward polarization throughout the $BaTiO_3$ thin film (apart from the top Ba-O dead layer) and not simply a complex surface relaxation. Notably, the ferroelectric distortion (δ_{FE}) values for the first Ti-O_2 and second Ba-O and Ti-O_2 layers (Table II) are, within the uncertainties of analysis, close to the bulk ferroelectric values.

The observation of a polar structural distortion, and hence polarization, in 4–10 ML films of $BaTiO_3$ is rather surprising. For metal-ferroelectric-metal heterostructures, the critical thickness is limited by the depolarizing field of the surface charge and was predicted to be 6 ML for $BaTiO_3$,[11] and is further reduced to 3 ML if the propagation of zone-center mode in the electrode is taken into account.[12] However, these mechanisms are applicable only to ferroelectric layers between metal electrodes, which screen the induced charge. In the experiments we have described, no top electrode is present. Alternate mechanisms for screening, which could

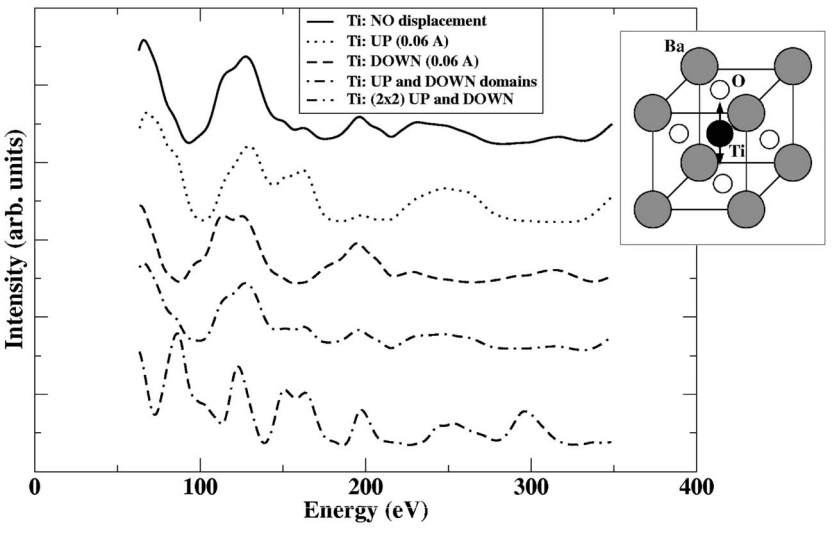

FIG. 5. Calculated LEED *I-V* curves for cubic $BaTiO_3(001)$ in five distinct situations: Ti centered (no displacement), Ti displaced up (0.06 Å), Ti displaced down (0.06 Å), a combination of Ti displacement up and down in domains (0.06 Å, 50%, and 50%), and a (2×2) structure with up and down Ti displacements (0.06 Å).

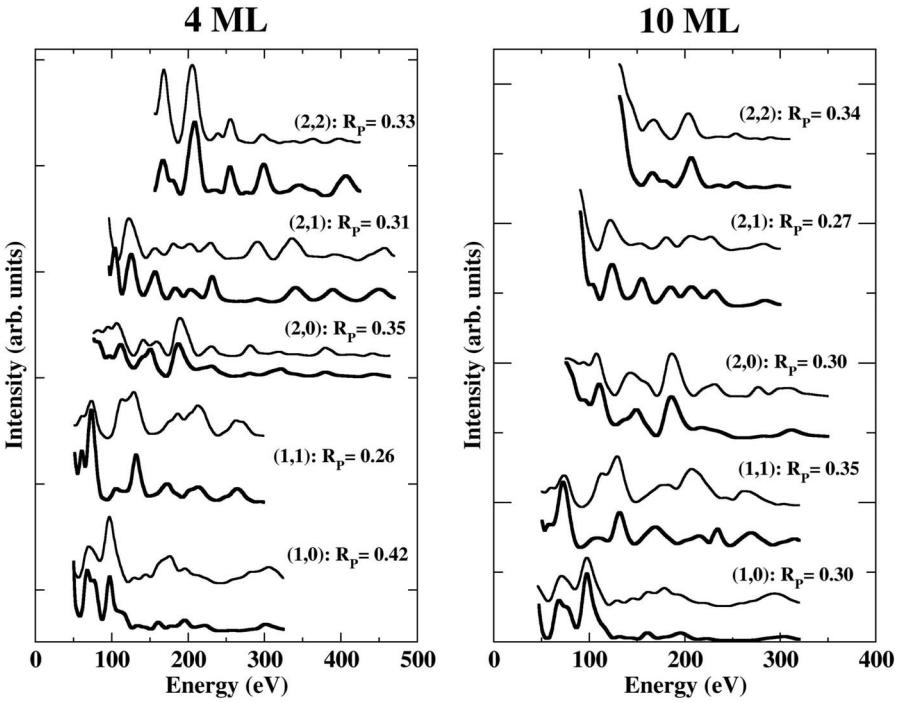

FIG. 6. Comparison between several experimental measurements (thick) and calculated intensities (thin) for the best-fit structure found for the 4 and 10 ML systems.

contribute to polarization stability, include surface chemisorption and surface charging from the LEED electron beam, supplying, on average, 1 electron per surface unit cell for every few seconds. Neither of these appears likely; the UHV conditions and LEED sensitivity rule out adsorbates other than hydrogen, and the lifetime of electrons on the surface due to leakage currents through a film as thin as 4 or 10 layers is limited.

A better case can be made that the polar state in these ultrathin films is determined by intrinsic electrostatic boundary conditions. First, the observation of a single domain orientation, polarized vertically toward the surface, follows from the electrostatic asymmetry between the bottom ($SrRuO_3$) and top (vacuum) electrodes. A single "monodomain" orientation has been previously observed on thicker ferroelectric films.[5,10] Second, stability of a polarized state in such thin films, despite the depolarizing field, and the presence of an unpolarized surface layer can be explained by the energetics of the surface. First-principles calculations from Meyer and Vanderbilt[13] and earlier by Padilla and Vanderbilt[34] have shown that the top layer in BaO-terminated surface of bulk $BaTiO_3$ is reconstructed to form a corrugated surface even in the unpolarized bulk phase, i.e., to minimize structural energy independent of internal fields. Their work predicts that even at zero internal field (in practice this is achieved computationally by setting the external field to zero) the surface of $BaTiO_3$ is corrugated to minimize strain energy. This corrugation creates a dipole that points into the surface with magnitude about 20% that of the bulk ferroelectric phase[13,34] and thus has the opposite direction than the

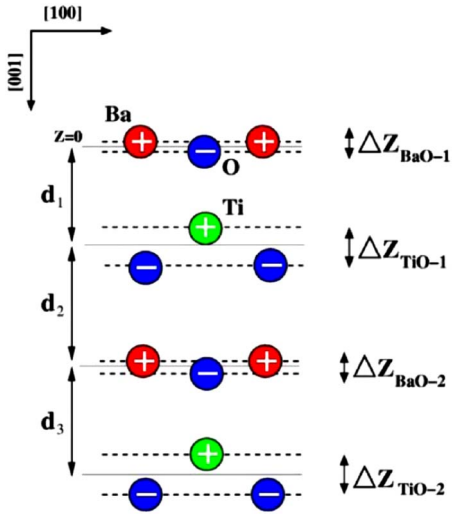

FIG. 7. (Color online) Best-fit surface structure obtained for the 4 and 10 ML $BaTiO_3$ thin films. The internal rumple in first and second Ba-O ($\Delta Z_{BaO\text{-}1}$ and $\Delta Z_{BaO\text{-}2}$) and Ti-O_2 ($\Delta Z_{TiO\text{-}1}$ and $\Delta Z_{TiO\text{-}2}$) layers, as well as the interlayer distances (d_1,d_2.d_3), are schematically presented. The interlayer distances are defined as the distance between the midpoint of one layer to the midpoint of the next consecutive layer.

TABLE I. Vertical rumple in the first and second Ba-O and Ti-O_2 layers, as obtained from the best structures found for the 4 and 10 ML thin films (Fig. 3). The d_1, d_2, and d_3 parameters correspond, respectively, to the interlayer distances, as shown in Fig. 7.

	4 ML (R_p=0.303±0.030)	10 ML (R_p=0.318±0.040)
$\Delta Z_{BaO\text{-}1}$	(0.034±0.070)Å	(0.022±0.080)Å
$\Delta Z_{TiO\text{-}1}$	(0.140±0.070)Å	(0.157±0.080)Å
$\Delta Z_{BaO\text{-}2}$	(0.056±0.110)Å	(0.118±0.110)Å
$\Delta Z_{TiO\text{-}2}$	(0.140±0.140)Å	(0.120±0.140)Å
d_1	(1.91±0.13)Å	(1.93±0.15)Å
d_2	(2.17±0.18)Å	(2.21±0.19)Å
d_3	(1.98±0.24)Å	(1.99±0.25)Å

TABLE II. Ferroelectric distortion (δ_{FE}) (in units of lattice constant ***c***) for the first and second BaO and TiO_2 surface layers. Experimental (Ref. 31) and theoretical (Ref. 34) bulk values are 0.0240 and 0.0232 for δ_{FE}(BaO) and 0.0285 and 0.0278 for $\delta_{FE}(TiO_2)$.

	4 ML	10 ML
δ_{FE}(BaO)-1	(0.008 ± 0.019)	(0.005 ± 0.019)
$\delta_{FE}(TiO_2)$-1	(0.034 ± 0.017)	(0.038 ± 0.019)
δ_{FE}(BaO)-2	(0.014 ± 0.027)	(0.028 ± 0.026)
$\delta_{FE}(TiO_2)$-2	(0.034 ± 0.034)	(0.029 ± 0.033)

dipoles we observed in second and deeper layers. Meyer and Vanderbilt found that when bulk polarization was incorporated, the dipole moments in the surface layers were modified relative to the bulk layers by the inward-oriented surface dipoles. Consequently, the nearly zero corrugation we observe in the outermost dead layer is a result of the competing inward dipole from surface energy and outward dipole from the internal electric fields. The result is an efficient compensation mechanism for the depolarization field.

V. CONCLUSION

The presence of polarization charges and the associated depolarization field controls the physical behavior of ferroelectrics. The pathway for minimization of the electrostatic energy chosen by the material—domain formation, screening by adsorbates or electrodes, surface band bending and formation of depletion layers, or changes in surface stoichiometry—depends on both thermodynamic and kinetic factors controlling the screening process. In theoretical models, both density functional theory and Landauer-Ginsburg-Devonshire formalism, only some of these mechanisms have been taken into account to date. Without correct models, these theories cannot determine what actually happens at a realistic surface.

This study reports the atomic structure on the $BaTiO_3$ surface under conditions where external environment (water adsorption, etc.) is controlled. Our work shows that surface structure and environment can determine the polarization direction and stability in ultrathin films. By providing evidence of polarization in 4 and 10 layer $BaTiO_3$ films, our research reveals that the true minimum film thickness for ferroelectric or ferroic behavior is still unknown. Loss of symmetry at the surface allows reconstructions that can compensate surface charge and the associated depolarizing field. In the $BaTiO_3$ films examined here, combined forces of surface stress and film polarization produce a surface dead layer with little polarization. For films thicker than those studied here, charge compensation by ferroelectric domain formation eventually becomes energetically preferred, although this may require hundreds of layers, at which point we predict a dead layer in domains parallel to the surface normal and an enhanced dipole in the outermost layer of inwardly oriented domains. In general, we observe that surface structure will even be more influential as studies explore thinner ferroelectric films and controlled environments with *in situ* characterization by surface sensitive techniques will be vital.

ACKNOWLEDGMENTS

Research was sponsored by the Division of Materials Science and Engineering with contributions (APB, EWP) to the growth and LEED *I-V* experiments from the Center For Nanophase Materials Sciences Division, under the Division of Scientific User Facilities, at Oak Ridge National Laboratory, for the U. S. Department of Energy. We would like to acknowledge J. Rundgren's (Royal Institute of Technology, Sweden) help with calculation of phase shifts.

*Corresponding author. baddorfap@ornl.gov

[1] M. E. Lines and A. M. Glass, *Principles and Applications of Ferroelectrics and Related Phenomena* (Clarendon, Oxford, 1977).
[2] C. Kittel, *Introduction to Solid State Physics* (Chapman and Hall, London, 1956).
[3] D. D. Fong, A. M. Kolpak, J. A. Eastman, S. K. Streiffer, P. H. Fuoss, G. B. Stephenson, C. Thompson, D. M. Kim, K. J. Choi, C. B. Eom, I. Grinberg, and A. M. Rappe, Phys. Rev. Lett. **96**, 127601 (2006).
[4] S. V. Kalinin, C. Y. Johnson, and D. A. Bonnell, J. Appl. Phys. **91**, 3816 (2002).
[5] D. D. Fong, C. Cionca, Y. Yacoby, G. B. Stephenson, J. A. Eastman, P. H. Fuoss, S. K. Streiffer, C. Thompson, R. Clarke, R. Pindak, and E. A. Stern, Phys. Rev. B **71**, 144112 (2005).
[6] I. I. Naumov, L. Bellaiche, and H. Fu, Nature (London) **432**, 737 (2004).
[7] Y. Watanabe, M. Okano, and A. Masuda, Phys. Rev. Lett. **86**, 332 (2001).
[8] M. Krcmar and C. L. Fu, Phys. Rev. B **68**, 115404 (2003).
[9] D. D. Fong, G. B. Stephenson, S. K. Streiffer, J. A. Eastman, O. Auciello, P. H. Fuoss, and C. Thompson, Science **304**, 1650 (2004).
[10] Y. S. Kim, D. H. Kim, J. D. Kim, Y. J. Chang, T. W. Noh, J. H. Kong, K. Char, Y. D. Park, S. D. Bu, J. G. Yoon, and J. S. Chung, Appl. Phys. Lett. **86**, 102907 (2005).
[11] J. Junquera and P. Ghosez, Nature (London) **422**, 506 (2003).
[12] G. Gerra, A. K. Tagantsev, N. Setter, and K. Parlinski, Phys. Rev. Lett. **96**, 107603 (2006).
[13] B. Meyer and D. Vanderbilt, Phys. Rev. B **63**, 205426 (2001).
[14] A. Munkholm, S. K. Streiffer, M. V. Ramana Murty, J. A. Eastman, C. Thompson, O. Auciello, L. Thompson, J. F. Moore, and G. B. Stephenson, Phys. Rev. Lett. **88**, 016101 (2001).
[15] V. E. Henrich and P. A. Cox, *The Surface Science of Metal Oxides* (Cambridge, New York, 1994).
[16] S. K. Streiffer, J. A. Eastman, D. D. Fong, C. Thompson, A. Munkholm, M. V. Ramana Murty, O. Auciello, G. R. Bai, and G. B. Stephenson, Phys. Rev. Lett. **89**, 067601 (2002).

[17] N. Bickel, G. Schmidt, K. Heinz, and K. Müller, Phys. Rev. Lett. **62**, 2009 (1989).
[18] M. A. Van Hove, W. H. Weinberg, and C.-M. Chan, *Low-Energy Electron Diffraction Experiment, Theory and Surface Structure Determination* (Springer-Verlag, Berlin, 1986).
[19] M. Kawasaki, K. Takahashi, T. Maeda, R. Tsuchiya, M. Shinohara, O. Ishiyama, T. Yonezawa, M. Yoshimoto, and H. Koinuma, Science **266**, 1540 (1994).
[20] G. Rijnders, D. H. A. Blank, J. Choi, and C. B. Eom, Appl. Phys. Lett. **84**, 505 (2004).
[21] J. Shin, Ph.D. thesis, University of Tennessee, 2007.
[22] W. Hong, H. N. Lee, M. Yoon, H. M. Christen, D. H. Lowndes, Z. G. Suo, and Z. Y. Zhang, Phys. Rev. Lett. **95**, 095501 (2005).
[23] J. Shin, S. V. Kalinin, A. Y. Borisevich, E. W. Plummer, and A. P. Baddorf, Appl. Phys. Lett. **91**, 202901 (2007).
[24] P. D. Nellist and S. J. Pennycook, Ultramicroscopy **78**, 111 (1999).
[25] V. B. Nascimento, R. G. Moore, J. Rundgren, J. Zhang, L. Cai, R. Jin, D. G. Mandrus, and E. W. Plummer, Phys. Rev. B **75**, 035408 (2007).
[26] J. B. Pendry, J. Phys. C **13**, 937 (1980).
[27] T. Loucks, *Augmented Plane Wave Method* (Benajamin, New York, 1976).
[28] J. Rundgren, Phys. Rev. B **68**, 125405 (2003).
[29] S. Müller, A. Kinne, M. Kottcke, R. Metzler, P. Bayer, L. Hammer, and K. Heinz, Phys. Rev. Lett. **75**, 2859 (1995).
[30] S. Walter, V. Blum, L. Hammer, S. Müller, K. Heinz, and M. Giesen, Surf. Sci. **458**, 155 (2000).
[31] J. Harada, T. Pedersen, and Z. Barnea, Acta Crystallogr., Sect. A: Cryst. Phys., Diffr., Theor. Gen. Crystallogr. **26**, 336 (1970).
[32] http://www.sitp.lbl.gov
[33] K. J. Choi, M. Biegalski, Y. L. Li, A. Sharan, J. Schubert, R. Uecker, P. Reiche, Y. B. Chen, X. Q. Pan, V. Gopalan, L. Q. Chen, D. G. Schlom, and C. B. Eom, Science **306**, 1005 (2004).
[34] J. Padilla and D. Vanderbilt, Phys. Rev. B **56**, 1625 (1997).